LOCKHEED MARTIN ENERGY RESEARCH LIBRARIES

3 4456 0515407 0

ORNL-4803

cy. 1

TUNGSTEN NEUTRON ELASTIC- AND INELASTIC-SCATTERING CROSS SECTIONS FROM 4.34 TO 8.56 MeV

W. E. Kinney

F. G. Perey

OAK RIDGE NATIONAL LABORATORY
CENTRAL RESEARCH LIBRARY
DOCUMENT COLLECTION
LIBRARY LOAN COPY
DO NOT TRANSFER TO ANOTHER PERSON
If you wish someone else to see this document, send in name with document and the library will arrange a loan.
UCN-7969
(3 3-67)

OAK RIDGE NATIONAL LABORATORY

OPERATED BY UNION CARBIDE CORPORATION • FOR THE U.S. ATOMIC ENERGY COMMISSION

Printed in the United States of America. Available from
National Technical Information Service
U.S. Department of Commerce
5285 Port Royal Road, Springfield, Virginia 22151
Price: Printed Copy $4.00; Microfiche $0.95

This report was prepared as an account of work sponsored by the United States Government. Neither the United States nor the United States Atomic Energy Commission, nor any of their employees, nor any of their contractors, subcontractors, or their employees, makes any warranty, express or implied, or assumes any legal liability or responsibility for the accuracy, completeness or usefulness of any information, apparatus, product or process disclosed, or represents that its use would not infringe privately owned rights.

ORNL-4803
UC-34 — Physics

Contract No. W-7405-eng-26

Neutron Physics Division

TUNGSTEN NEUTRON ELASTIC- AND INELASTIC-SCATTERING CROSS SECTIONS FROM 4.34 TO 8.56 MeV

W. E. Kinney and F. G. Perey

MAY 1973

OAK RIDGE NATIONAL LABORATORY
Oak Ridge, Tennessee 37830
operated by
UNION CARBIDE CORPORATION
for the
U.S. ATOMIC ENERGY COMMISSION

LOCKHEED MARTIN ENERGY RESEARCH LIBRARIES

3 4456 0515407 0

Table of Contents

	Page No.
Introduction	1
Data Acquisition	1
Data Reduction	3
Results	5
Elastic Scattering and Inelastic Scattering to Low-Lying Levels	5
Inelastic Scattering to Level > 0.123 MeV	11
Conclusions	18
Acknowledgements	19
Appendix	27

TUNGSTEN NEUTRON ELASTIC- AND INELASTIC-SCATTERING CROSS SECTIONS FROM 4.34 TO 8.56 MeV

W. E. Kinney and F. G. Perey

ABSTRACT

Measured natural tungsten neutron elastic- and inelastic-scattering cross sections are presented and shown to be in good agreement with the results of others. An evaporation model of inelastic scattering was found to be applicable with nuclear temperatures in agreement with previous results but with total inelastic cross sections larger by as much as 20% than measured nonelastic cross sections. ENDF/B W (Mat 1060-63) elastic angular distributions agree with our data at angles less than 50° but do not at larger angles. The ENDF/B nuclear temperatures are 10-15% lower than experimental temperatures.

INTRODUCTION

We present neutron elastic- and inelastic-scattering cross sections for natural tungsten at 4.34, 4.92, 6.44, 7.54 and 8.56 MeV. To assist in the evaluation of our data, we briefly discuss our data acquisition and reduction techniques.

For the purposes of discussion, we present our data in graphical form where we compare with the results of others and with ENDF/B (Evaluated Neutron Data File B). Tables of our numerical values of the cross section are given in the appendix.

DATA ACQUISITION

The data were obtained with conventional time-of-flight techniques. Pulsed (2MHz), bunched (~1 nsec full width at half maximum, FWHM) deuterons accelerated by the ORNL Van de Graaff's interacted with deuterium in a gas cell to produce neutrons by the $D(d,n)^3He$ reaction. The gas cells, of length 1 and 2 cm, were operated at pressures of approximately 1.5 atm and gave neutron energy resolutions of the order of $\pm$ 60 keV.

The neutrons were scattered from a solid right circular cylindrical sample of natural tungsten, 0.953 cm diameter and 2.56 cm high, placed approximately 10 cm from the gas cells when the detector angles were greater than 25°. For smaller detector angles the cell-to-sample distance had to be increased to as much as 30 cm in order to shield the detector from neutrons coming directly from the gas cells.

The scattered neutrons were detected by 12.5-cm-diam NE-213 liquid scintillators optically coupled to XP-1040 photomultipliers. The scintillators were normally 2.5 cm thick. Data were taken with three detectors simultaneously. Flight paths were approximately 5 m with the detector angles ranging from 15 to 140°. The gas-cell neutron production was monitored by a time-of-flight system which used a 5-cm-diam by 2.5-cm-thick NE-213 scintillator viewed by a 58-AVP photomultiplier placed about 4 m from the cell at an angle of 55° with the incident deuteron beam.

For each event a PDP-7 computer was given the flight time of a detected recoil proton event with reference to a beam pulse signal, the pulse height of the recoil proton event, and identification of the detector. The electronic equipment for supplying this information to the computer consisted, for the most part, of standard commercial components. The electronic bias, determined by deterioration of gamma-neutron discrimination, was set at approximately 700-keV neutron energy.

The detector efficiencies were measured by (n,p) scattering from a thin (6-mm-diam) polyethylene sample and by detecting source $D(d,n)^{3}He$ neutrons . Both interactions gave results which agreed with each other and which yielded efficiency vs energy curves that compared well with calculations.[1]

DATA REDUCTION

Central to the data reduction process was the use of a light pen with the PDP-7 computer oscilloscope display programs to extract peak areas from spectra. The light pen made a comparatively easy job of estimating errors in the cross section caused by extreme but possible peak shapes.

The reduction process started by normalizing a sample-out to a sample-in time-of-flight spectrum by the ratio of their monitor neutron peak areas, subtracting the sample-out spectrum, and transforming the difference spectrum into a spectrum of center-of-mass cross section vs excitation energy. This transformation allowed ready comparison of spectra taken at different angles and incident neutron energies by removing kinematic effects. It also made all singlet peaks have approximately the same shape and width regardless of excitation energy (in a time-of-flight spectrum, singlet peaks change shape drastically with flight time). A spectrum of the variance based on the counting statistics of the initial data was also computed.

The transformed spectra were read into the PDP-7 computer and the peak stripping was done with the aid of the light pen. A peak was stripped by drawing a background beneath it, subtracting the background, and calculating the area, centroid, and FWHM of the difference. The variance spectrum was used to compute a counting statistics variance corresponding to the stripped peak. Peak stripping errors due to uncertainties in the residual background under the peaks or to the tails of imperfectly resolved nearby peaks could be included with the other errors by stripping the peaks several times corresponding to high, low, and best estimates of this background. Although somewhat subjective, the low and high estimates of the cross sections were

identified with 95% confidence limits; these, together with the best estimate, defined upper and lower errors due to stripping. When a spectrum was completely stripped, the output information was written on magnetic tape for additional processing by a large computer.

Inelastic cross sections were sufficiently isotropic so that finite sample corrections could be made at each angle independently of results at other angles. Correction of the elastic cross section, however, had to await the reduction of the entire angular distribution before the finite sample effects could be treated. The corrections were performed according to semianalytic recipes whose constants were obtained from fits to Monte Carlo results.[2] The corrections are largest in the first minimum of the elastic differential cross section, amounting to ~30% in the first minimum at 4.34 MeV but decreasing to ~15% at 8.56 MeV.

The final error analysis included uncertainties in the geometrical parameters (scatterer size, gas cell to scatterer distance, flight paths, etc.) and uncertainties in the finite sample corrections.

The ground state was fitted by least squares to a Legendre series:

$$\sigma(\mu = \cos\theta) = \sum_{\ell=0} \frac{2\ell+1}{2} a_\ell P_\ell(\mu),$$

the points being weighted by the inverse of their variances. In order to prevent the fit from giving totally unrealistic values outside the angular range of our measurements, we resorted to the inelegant but workable process of adding three points equally spaced in angle between the largest angle of measurement and 175°. The differential cross sections at the added points were chosen to approximate the diffraction pattern at large angles, but were assigned 50% errors.

RESULTS

Elastic Scattering and Inelastic Scattering to Low-Lying Levels

Differential cross sections for predominantly elastic scattering are shown in Figure 1 along with the Legendre fits we used to integrate the distributions over angle. Our resolution was not sufficiently good to separate inelastic scattering to levels of energy up to 0.123 MeV from elastic scattering. On the basis of the counts in the time-of-flight spectra just below the 'elastic-scattering' peak, assuming a similar contribution for inelastic scattering to levels not resolved from the 'elastic-scattering' peak, we estimate that the unresolved inelastic levels contribute less than 6% to the 'elastic-scattering' data.

Our differential cross sections are compared with those of others in Figure 2. The ENDF/B-III+ elastic differential cross sections for Mat 1060 through 1063 (^{182}W, ^{183}W, ^{184}W, and ^{186}W, respectively) are also shown. These were obtained by combining the information for the isotopes ^{182}W, ^{183}W, ^{184} and ^{185}W, MAT 1060 through 1063.

The ENDF/B Legendre coefficients for natural tungsten were determined by

$$f_\ell = \frac{\sum_{i=1}^{4} a_\ell^i \, p_i \, \sigma_{si}}{\sum_{i=1}^{4} p_i \, \sigma_{si}} \qquad (1)$$

where

f_ℓ = the ℓth Legendre coefficient for natural tungsten,

a_ℓ^i = the ℓth Legendre coefficient for the ith isotope,

p_i = the natural isotopic abundance for the ith isotope,

σ_{si} = the ENDF/B-III angle-integrated elastic-scattering cross section for the ith isotope.

+Tungsten is currently being reevaluated by P. F. Rose at Atomics International.

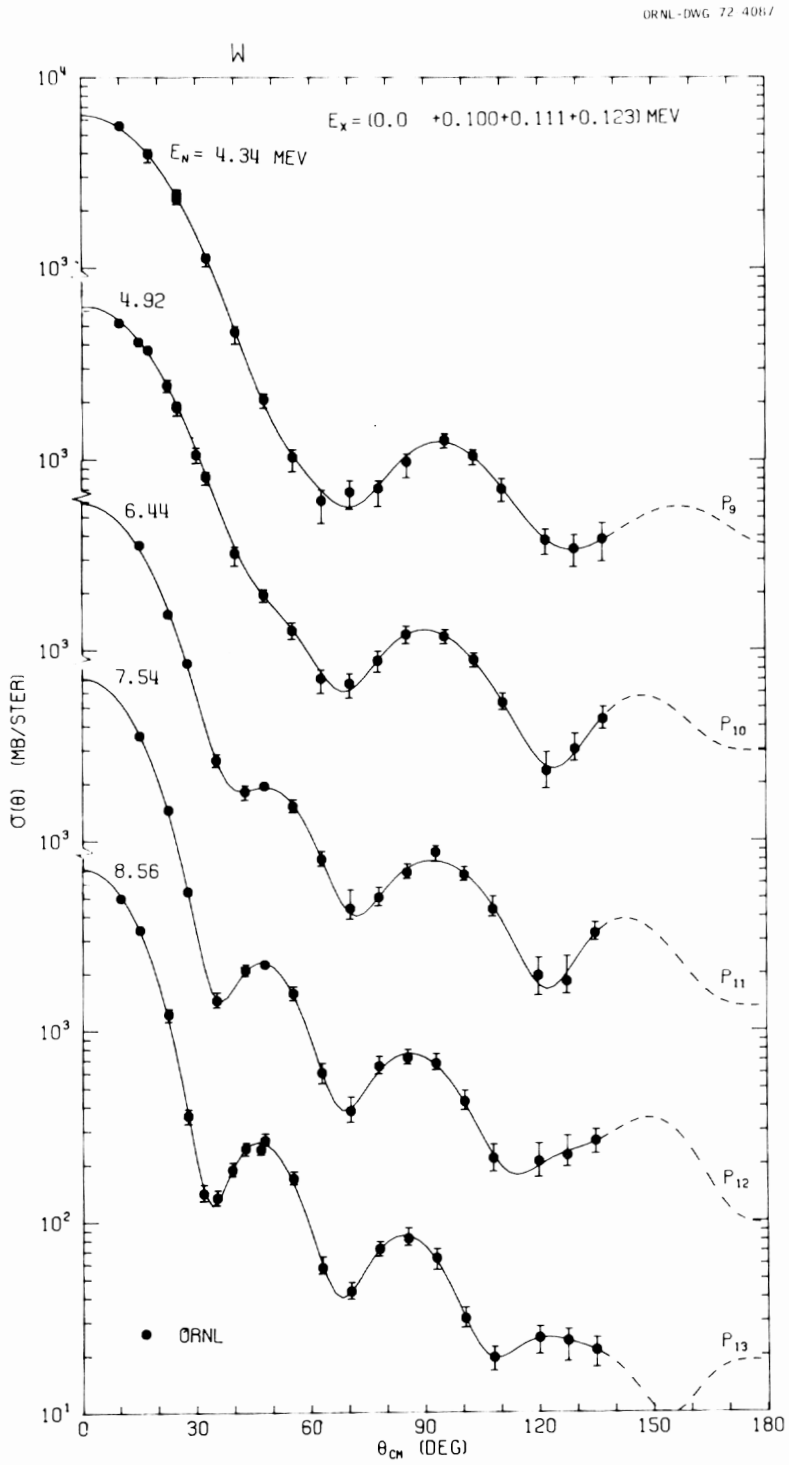

Fig. 1. Our neutron differential cross sections for natural tungsten for elastic scattering and inelastic scattering to levels $\leq$ 0.123 MeV. The curves are Legendre fits to the data.

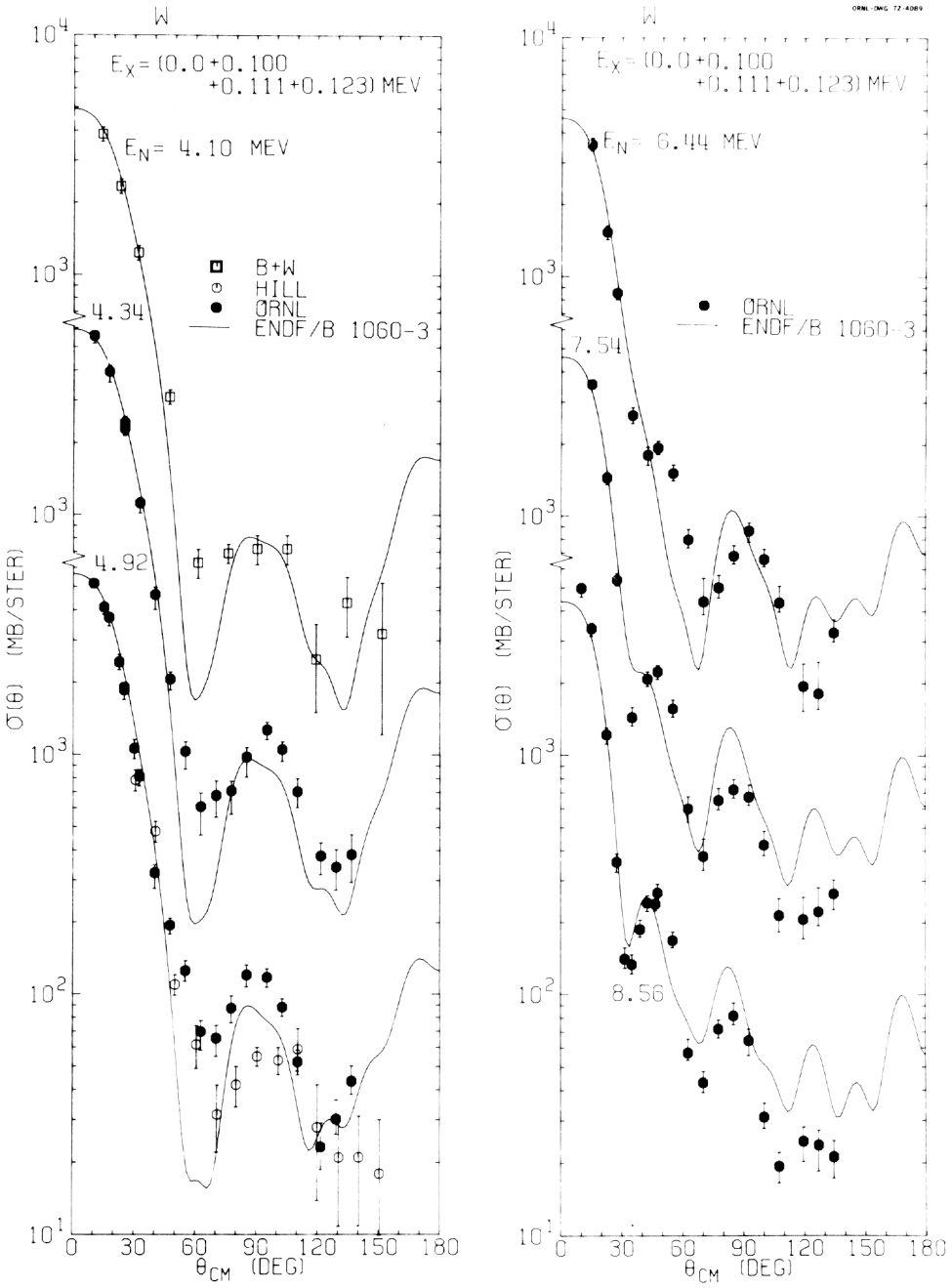

Fig. 2. Our neutron differential cross sections for natural tungsten for elastic scattering and inelastic scattering to levels $\leq$ 0.123 MeV together with the data of Beyster and Walt (B&W) and Hill. The curves are ENDF/B elastic differential cross sections for the tungsten isotopes (Mat 1060 through Mat 1063) combined with natural isotopic abundances and normalized to the experimental integrals.

The ENDF/B angular distributions were normalized to experimental integrated elastic-scattering cross sections.

Our results appear to be consistent with those of Beyster and Walt (B+W)[3] at 4.10 $\pm$ 0.04 MeV. At angles less than 60°, our data agree with that of Hill[3] who measured at 5.0 $\pm$ 0.1 MeV; but our data are about a factor of two higher in the second maximum. The ENDF/B-III angular distributions agree within errors at angles less than 50°, except possibly at 8.56 MeV. At angles greater than 60°, however, ENDF/B-III angular distributions rarely agree with the data within experimental errors and also show structure not evident in the data.

An interesting comparison of our elastic differential cross sections for natural tungsten (Z=74,A=193.6) is made with similar data of Holmqvist and Wiedling[6] for natural tantalum (Z=73,A=181) in Figure 3. The curves are our Legendre fits to our data and Holmqvist's and Wiedling's Legendre fits to their data. It would be expected that neighboring nuclei in this mass region should have very similar differential elastic-scattering cross sections and, although our data integrate to values approximately 20% higher than do the data of Holmqvist and Wiedling, the shapes are very much the same. The evolution of what at 8.56 MeV is the first minimum is most striking while the occurrence of the other minima at smaller angles with increasing energy is also evident.

Our angle-integrated differential cross sections for elastic scattering and inelastic scattering to levels $\leq$ 0.123 MeV are compared with the elastic cross section of ENDF/B in Figure 4. The evaluation lies within our errors except at 6.44 MeV where it is 12% higher.

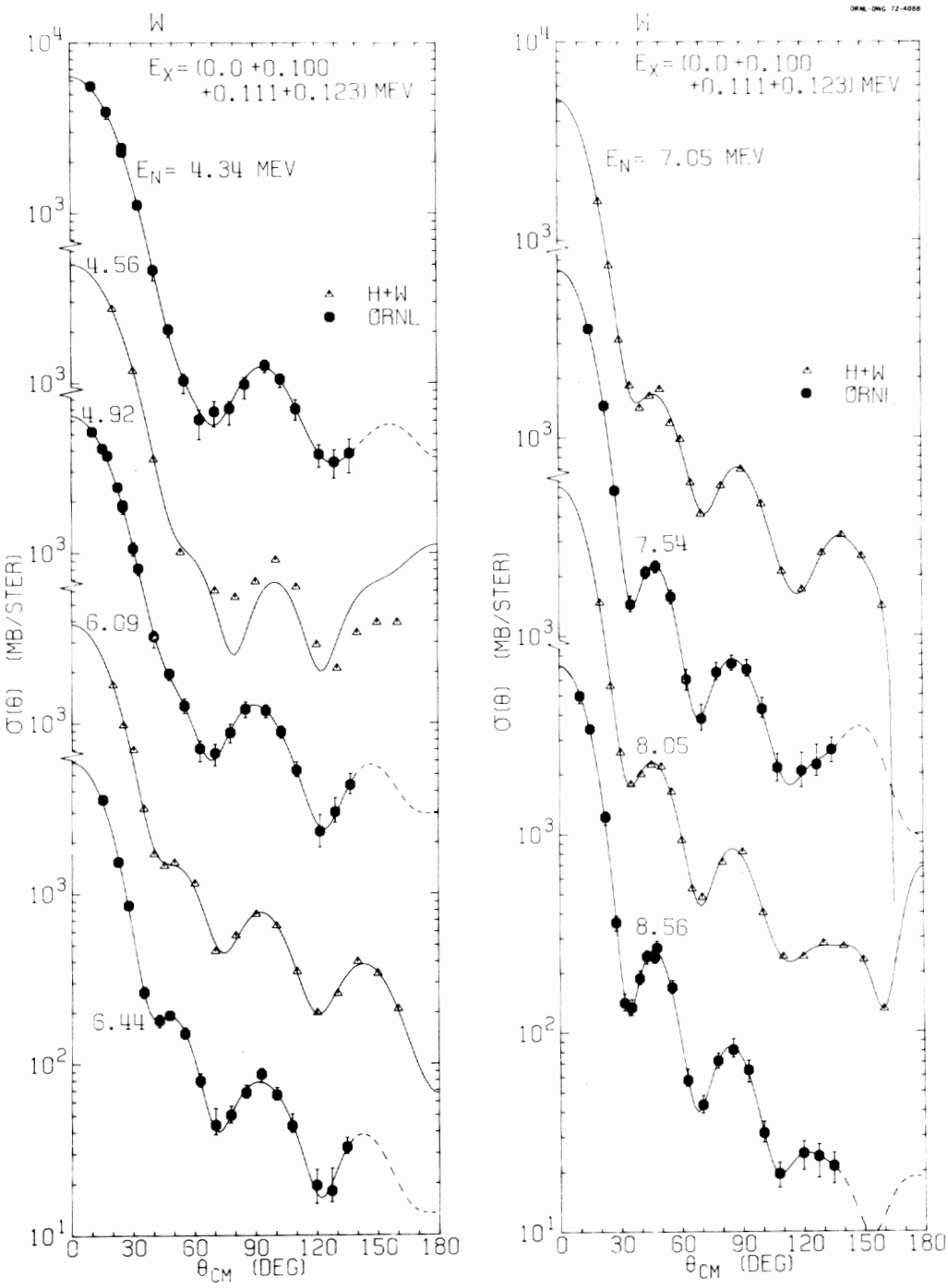

Fig. 3. Our neutron differential cross sections for natural tungsten for elastic scattering and inelastic scattering to levels $\leq$ 0.123 MeV compared with neutron differential cross sections of Holmqvist and Wiedling (H&W) for natural tantalum.

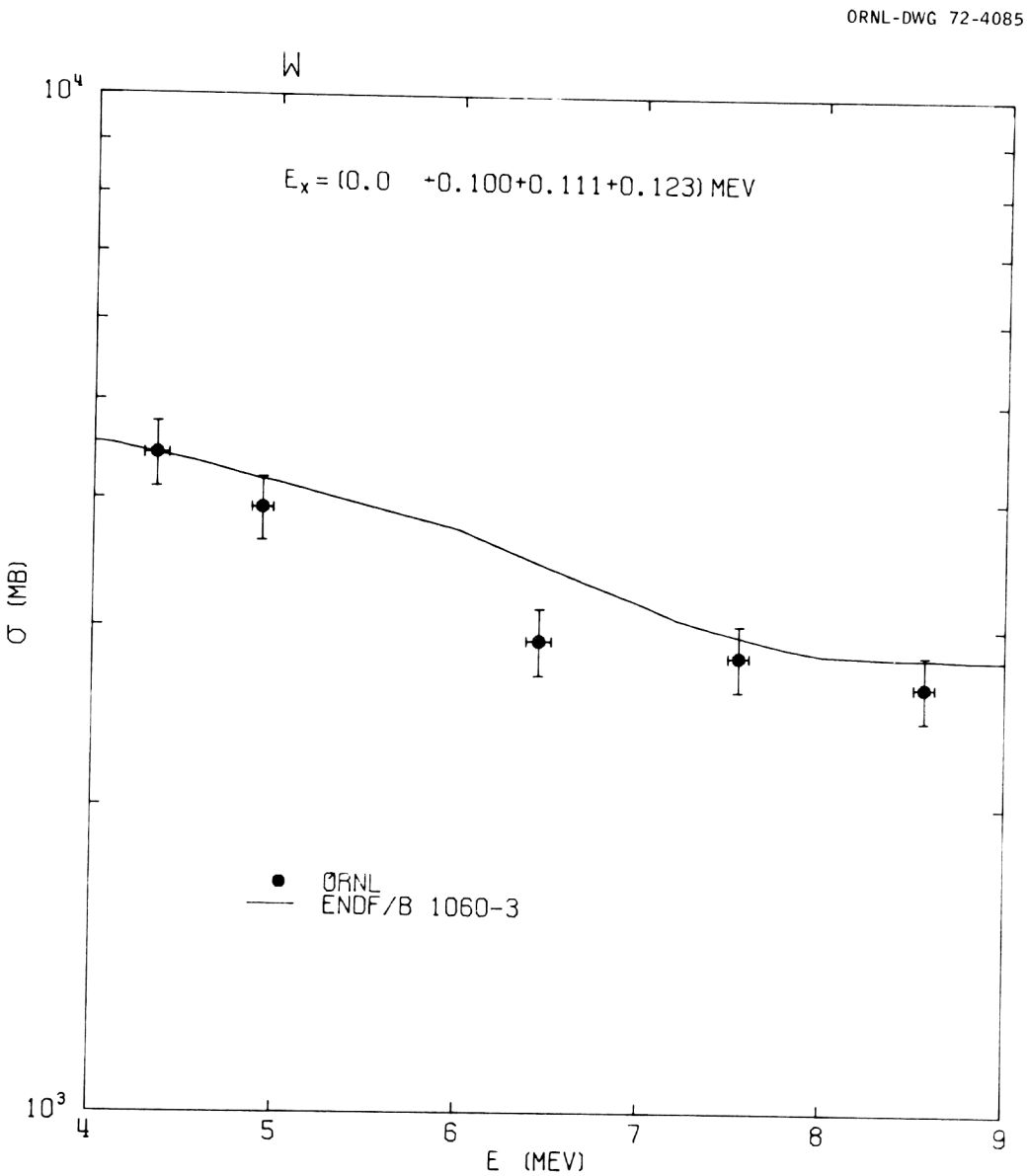

Fig. 4. Our angle-integrated differential cross sections for natural tungsten for elastic scattering and inelastic scattering to levels $\leq$ 0.123 MeV compared with ENDF/B Mat 1060-63.

Inelastic Scattering to Levels > 0.123 MeV

The relatively high energy level density of the tungsten isotopes, the presence of four isotopes in natural tungsten with abundances from 14 to 30%, and our resolution of ~ $\pm$60 keV combined to prevent our resolving inelastic scattering into cross sections for scattering to particular levels or small groups of few levels. Rather, inelastic scattering appeared as scattering to a continuum of levels as shown in Figure 5 where our angle-averaged double differential cross sections for inelastic scattering are plotted versus excitation energy for our five incident neutron energies.

As the incident neutron energy increases the number of levels open for deexcitation of the compound nucleus formed increases, decreasing the probability of inelastic scattering to a particular level. In fact, scattering to the lower lying levels in the tungsten isotopes becomes so small at the higher incident neutron energies so as to become of the order of magnitude of the background. Rather than quote very large, and possibly meaningless, errors for the inelastic-scattering cross sections to these low-lying levels, we only report inelastic-scattering cross sections to the continuum at increasingly higher excitation energies as the incident neutron energy increases.

An evaporation model has been applied by others to tungsten continuum inelastic scattering to obtain nuclear temperatures.[7,8]

In this model

$$\sigma(E,E') = KE'e^{-E'/T} \qquad (2)$$

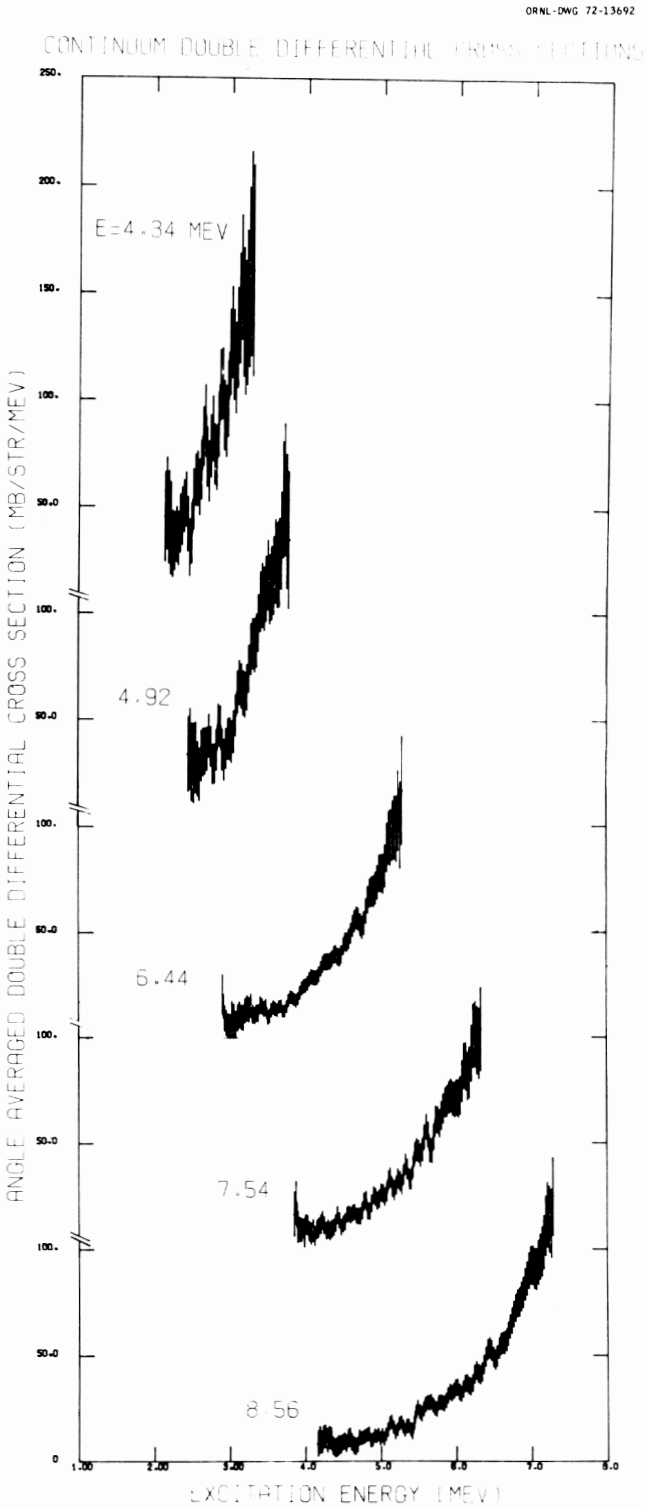

Fig. 5. Our angle-averaged double differential cross sections for inelastic scattering to the continuum.

where

$\sigma(E,E')$ = the cross section for scattering from neutron energy E to energy dE' about E',

K = a proportionality constant,

T = the nuclear temperature.

Figure 6 shows plots of $\sigma(E,E')/E'$ versus E' with least squares fits to the data. In the fitting only data with E' < 2 MeV were used for E = 4.34 and 4.92 MeV; E' < 2.5 MeV for E = 6.44 MeV; E' < 3 MeV for E = 7.54 and 8.56 MeV. The temperatures and their least square errors are indicated.

The nuclear temperatures deduced from our data are compared with those from other investigations[7,8] in Figure 7. The dotted line is a least squares fit to all the experimental points giving a dependence of temperature on incident neutron energy of

$$T = 0.223 + 0.055\ E$$

where

T = the temperature in MeV,

E = the incident energy in MeV.

The ENDF/B temperatures are given by the solid line and are seen to be 10-15% lower than the fit to experimental values.

The evaporation spectrum, Eq. (2), may be integrated to give a total inelastic-scattering cross section

$$\sigma_{in} = \iint \sigma(E,E')dE'\ d\Omega \simeq 4\pi KT^2, \qquad (3)$$

assuming an isotropic angular distribution. The constants K and T were obtained from the least square fits shown on Figure 6. The error on the

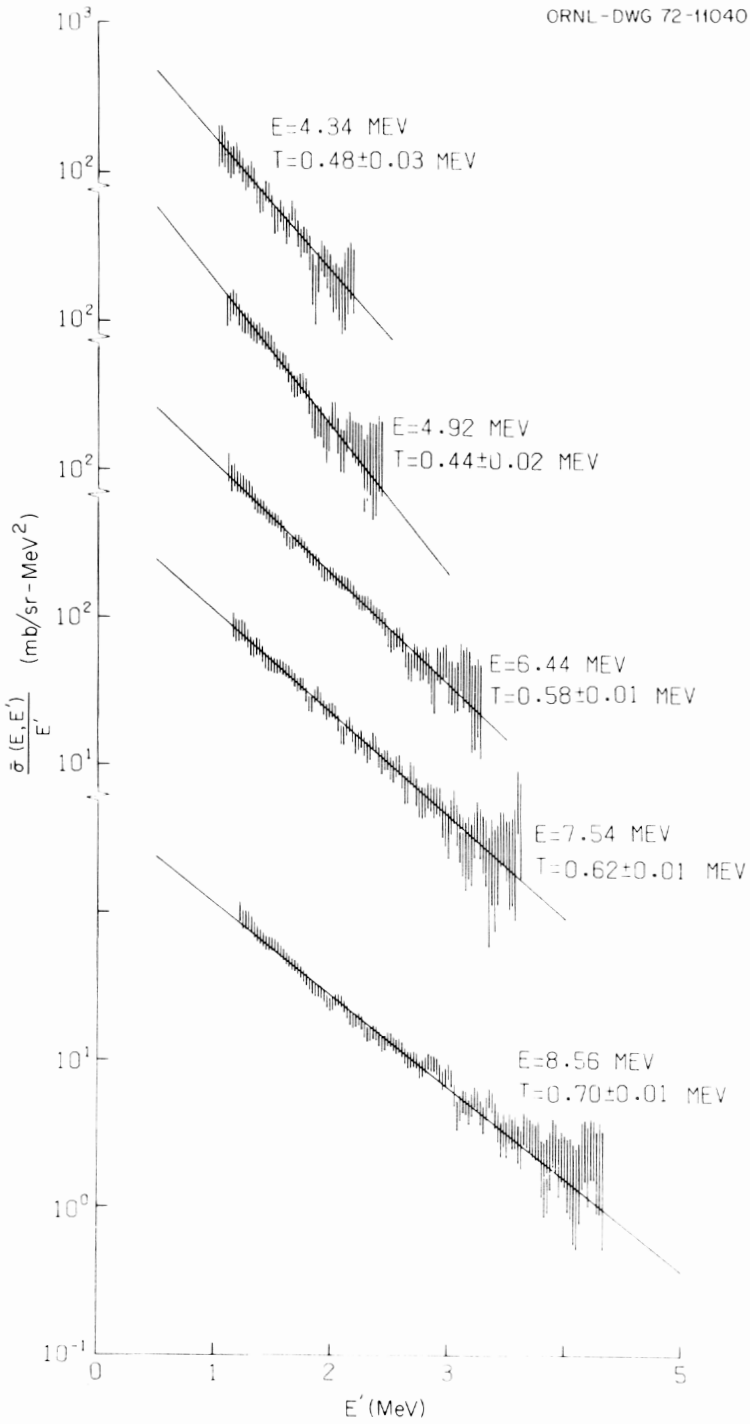

Fig. 6. Natural tungsten average neutron differential cross sections for scattering from energy E to scattered energy dE' about E' divided by E' versus E'. The straight lines are least squares fits to the data. T, the reciprocal of the plot of the best fit line to the data, is the nuclear temperature characterizing each spectrum.

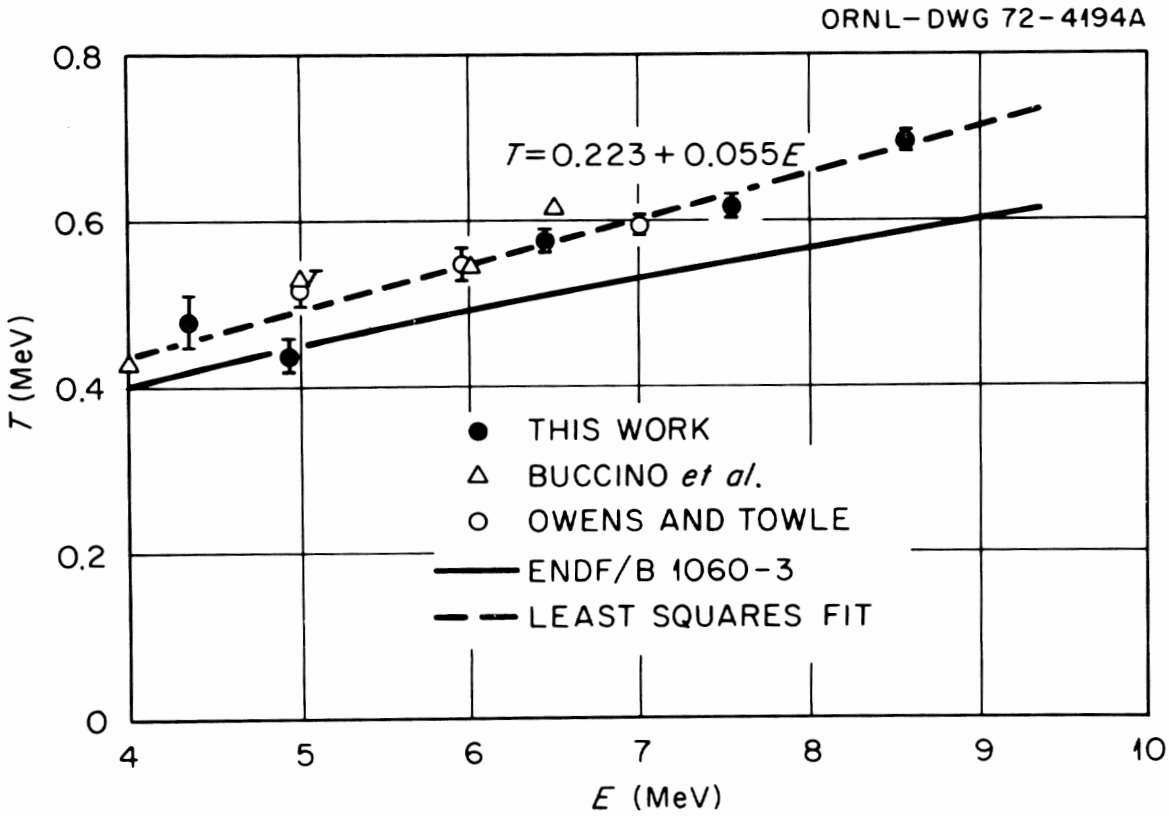

Fig. 7. Our nuclear temperatures, T, for natural tungsten versus incident energy E compared with results of others. The dotted line is a least squares fit to all the experimental data. The solid line, lying 10-15% below the dotted, is the ENDF/B temperature variation with energy.

total inelastic scattering cross section computed using Eq. (3) is larger than the one derived only from the errors on K and T, obtained from the fits of Figure 6, since one is assuming that the unobserved part of the spectrum at low and high energies obey the same evaporation law. At the lower incident neutron energies of 4.34 and 4.92 MeV the use of Eq. (3) is very unsatisfactory since the largest contribution to the integrated cross section would come from the unmeasured energy region of the spectrum. At these two low energies we believe that the inelastic spectra can only be used to obtain an estimate on the temperature T, to characterize the measured part of the spectrum and should not be used to derive a meaningful total inelastic cross section.

Table I lists the values we obtain from our data using Eq. (3) at 6.44, 7.55 and 8.56 MeV. The errors shown only include the contributions due to the uncertainties on K and T from the least squares fit to the measured spectra. For comparison we also show the values of the nonelastic cross sections obtained by subtracting our total elastic-scattering cross sections from total cross sections,[9] as well as nonelastic cross sections from Ref. 10. The results of Owens and Towle[8] for total inelastic scattering and the values ENDF/B 1060 for nonelastic scattering are also included. At the neutron energies given in Table I, the nonelastic-scattering cross sections are only the sum of the inelastic-scattering and capture cross sections. Since the capture cross sections are relativley small in this energy region, a few millibarns, the nonelastic cross sections should be approximately equal to the inelastic cross sections. Table I shows a systematic discrepancy between nonelastic and inelastic cross sections. All of the data given for inelastic-scattering cross sections in this table were obtained by using Eq. (3).

Table I. A Comparison of Tungsten Total Inelastic and Nonelastic Cross Sections. All Cross Sections are Given in Barns.

E,MeV	σ_{non}^{a}	σ_{non}^{b}	Total Inelastic	$\sigma_T - \sigma_S$	σ_T^{c}
5.00	2.6±0.3	2.53	2.94±0.15[d]		
6.00	2.5±0.3	2.34	2.89±0.13[d]		
6.44	2.5±0.3	2.28	2.6 ±0.3	2.5±0.2	5.40±0.1
7.00	2.5±0.3	2.32	2.87±0.17[d]		
7.54	2.5±0.3	2.32	2.7 ±0.3	2.3±0.2	5.13±0.1
8.56	2.5±0.3	2.29	3.0 ±0.3	2.4±0.2	5.08±0.1

[a] Ref. 10 (BNL-325)

[b] ENDF/B 1060

[c] Ref. 9 (LASL evaluation)

[d] Ref. 8 (direct measurements)

For the data of Owens and Towle[8] and our 8.56 MeV results, too-large values of the inelastic cross sections are obtained from the use of Eq. (3). We have not investigated in detail this problem. It could be that the low-energy part of the inelastic spectrum, which we do not observe, has fewer neutrons than predicted by the evaporation law based on the temperature T determined at higher energies. Or more likely, the error estimate which we obtain on the integrals using Eq. (3) do not properly reflect the uncertainties in the data. Further experiments, with particular attention given to background reduction and determination, would be required to clear up this possible discrepancy. We believe in the meantime that the nonelastic cross sections obtained by subtracting the integrated elastic-scattering cross sections from the total cross sections are more reliable and their error estimates realistic.

CONCLUSIONS

The ENDF/B W (Mat 1060-63) elastic-scattering angular distributions are in agreement with our data at angles less than 50° but disagree at larger angles. The ENDF/B angle-integrated elastic cross sections, however, are in general agreement with our data.

Inelastic scattering to the continuum is adequately described by a simple evaporation model employing a nuclear temperature, but total inelastic cross sections obtained from integrating the evaporation spectrum are higher than measured noneleastic cross sections by as much as 20%. The ENDF/B Mat 1060-63 nuclear temperatures lie 10-15% below experimental values from 4 to 9 MeV.

ACKNOWLEDGMENTS

Many have contributed to this experimental program at one time or another and we would like to thank them for their contributions. In particular, we would like to acknowledge the help of J. K. Dickens, J. W. McConnell, J. A. Biggerstaff, A. M. Marusak, P. H. Stelson, C. O. LeRigoleur, and E. Hungerford.

REFERENCES

1. R. E. Textor and V. V. Verbinski, O5S: A Monte Carlo Code for Calculating Pulse Height Distributions Due to Monoenergetic Neutrons Incident on Organic Scintillators, ORNL-4160 (February 1968).

2. W. E. Kinney, Nucl. Instr. and Methods 83, 15 (1970).

3. M. Walt and J. R. Beyster, Phys. Rev. 98, 677 (1955).

4. P. F. Rose, Atomics International, P. O. Box 309, Canoga Park, California 91304, private communication.

5. R. W. Hill, Phys. Rev. 109, 2105 (1958).

6. B. Holmqvist and T. Wiedling, "Neutron Elastic Scattering Cross Sections. Experimental Data and Optical-Model Cross-Section Calculations," AKTIEBOLAGET ATOMENERGI Report AE-366 (June 1969).

7. S. G. Buccino, C. E. Hollandsworth, H. W. Lewis and P. R. Bevington, Nucl. Phys. 60, 17 (1964).

8. R. O. Owens and J. H. Towle, Nucl. Phys. A112, 337 (1968).

9. J. J. Devaney and P. G. Foster, Jr., An Evaluation of the Total Cross Section for Tungsten, LA-4928 (June 1972).

10. M. D. Goldberg, et al., Neutron Cross Sections, Volume 11C, Z = 61 to 87, BNL-325, Supplement 2 (August 1966).

APPENDIX

Tabulated Values of Natural W Neutron Elastic- and Inelastic-Scattering Cross Sections from 4.34 to 8.56 MeV

In the following tables we give our results for natural tungsten neutron elastic- and inelastic-scattering cross sections. We first tabulate the differential cross sections for elastic scattering including inelastic scattering to levels $\leq$ 0.123 MeV. The tabulated uncertainties are relative and do not include a $\pm$ 7% uncertainty in detector efficiency which is common to all points. The angle uncertainty is $\pm 1^{\circ}$. The uncertainty in integrated cross sections do include the $\pm$ 7% standard efficiency error.

Cross sections for inelastic scattering to levels > 0.123 MeV are given in the continuum tables as angle-averaged double-differential cross sections which are constant over 25 keV intervals as shown in Figure 5. The value in the Q_N column is the upper limit of the 25 keV interval in Q value (the lower limit of excitation energy). The continuum cross-section uncertainties do not include the $\pm$ 7% standard error in detector efficiency.

Table A1. A Table of Contents for the W Neutron Cross Section Tables

Quantity	Page No.
Elastic Scattering Plus Inelastic Scattering up to Levels $\leq$ 0.123 MeV	23 - 27
Continuum	28 - 34

SCATTERING OF 4.34 +OR-0.07 MEV NEUTRONS FROM W

LEVEL(S) 0.0 MEV KE1(14) 18 ANGLES
0.100
0.111
0.123

ANGLE CM	X-SEC. MB/STR	ERROR(0/0) +	-	RUN
MULTIPLE SCATTERING CORRECTION DONE				
10.08	5568.92	4.0	7.0	26701
17.62	3950.79	6.1	9.6	26705
25.14	2284.66	4.6	6.4	10401
25.15	2418.84	6.0	11.1	26703
32.68	1120.87	5.2	9.3	10405
40.21	463.98	7.2	13.4	10403
47.74	205.91	7.3	9.7	15501
55.26	103.15	9.5	15.8	15505
62.78	60.93	14.0	23.9	15503
70.30	67.82	14.7	18.7	10901
77.81	70.78	9.7	19.9	10905
85.31	97.76	9.7	17.4	10903
95.32	126.81	7.8	9.1	14401
102.81	105.06	7.6	10.6	14405
110.30	70.32	13.4	14.2	14403
121.77	37.97	13.7	16.4	12501
129.25	34.15	18.3	19.8	12505
136.73	38.48	21.4	23.6	12503

AVERAGE X-SEC 0.0 MB/STR 0 NOTE

INTEGRATED X-SEC 4432.75 MB ERROR 7.4 PER CENT

P 9 FIT

L	COEF.	ERROR(0/0)
0	705.49536	2.5
1	525.88184	3.0
2	422.14502	3.3
3	333.76416	3.4
4	241.92575	4.1
5	143.97351	5.6
6	79.75507	8.0
7	47.38870	10.7
8	21.09935	16.3
9	5.68121	40.4

SCATTERING OF 4.92 +OR-0.06 MEV NEUTRONS FROM W

LEVEL(S) 0.0 MEV KET(14) 21 ANGLES
0.100
0.111
0.123

ANGLE CM	X-SEC. MB/STR	ERROR(0/0) +	-	RUN
MULTIPLE SCATTERING CORRECTION DONE				
10.06	5164.44	3.9	5.2	25901
15.09	4115.61	4.6	6.7	24901
17.60	3727.87	4.6	7.9	25905
22.64	2431.48	7.4	7.4	24905
25.14	1863.92	6.0	9.2	25903
25.14	1909.34	4.5	5.3	9101
30.17	1061.56	8.9	9.6	24903
32.68	812.08	6.5	8.7	9105
40.20	322.76	8.1	14.0	9103
47.74	195.00	7.0	8.3	2201
55.26	126.19	10.1	10.0	2205
62.78	70.70	11.0	16.1	2203
70.30	66.46	12.9	15.7	3601
77.81	87.82	12.4	13.1	3605
85.32	120.61	10.3	10.8	3603
95.32	117.77	8.5	8.9	7201
102.81	88.66	8.4	8.3	7205
110.30	52.89	11.8	8.4	7203
121.77	23.23	25.6	19.1	6301
129.24	30.23	20.5	13.4	6305
136.72	43.49	15.9	11.8	6303

AVERAGE X-SEC 0.0 MB/STR 0 NOTE

INTEGRATED X-SEC 3923.41 MB ERROR 7.2 PER CENT

P10 FIT

L	COEF.	ERROR(0/0)
0	624.43066	1.9
1	460.44873	2.3
2	367.57446	2.5
3	296.88379	2.6
4	229.01265	3.0
5	151.29405	4.0
6	90.59291	5.7
7	62.68361	6.7
8	36.10461	9.3
9	14.85574	15.9
10	4.30727	37.3

SCATTERING OF 6.44 +OR-0.07 MEV NEUTRONS FROM W

LEVEL(S) 0.0 MEV KEY(14) 17 ANGLES
0.100
0.111
0.123

ANGLE CM	X-SEC. MB/STR	ERROR(0/0) +	-	RUN
MULTIPLE SCATTERING CORRECTION DONE				
15.08	3562.83	6.6	5.8	50502
22.63	1536.66	6.2	7.2	30502
27.65	853.64	4.7	6.1	50203
35.18	263.98	8.1	7.4	30203
42.71	180.24	8.1	9.2	10203
47.73	193.51	6.8	5.9	50187
55.26	151.49	8.6	6.9	30187
62.78	79.84	10.4	7.6	10187
70.30	43.85	25.6	11.8	50126
77.80	50.24	12.9	9.6	30126
85.31	68.24	10.6	7.3	10126
92.81	87.02	8.2	10.5	50142
100.31	66.03	10.5	6.8	30142
107.80	43.42	17.7	8.4	10142
119.77	19.49	24.3	21.5	50156
127.25	18.14	35.9	13.9	30156
134.72	32.60	13.8	8.4	10156

AVERAGE X-SEC 0.0 MB/STR 0 NOTE

INTEGRATED X-SEC 2912.43 MB ERROR 7.6 PER CENT

P11 FIT

L	COEF.	ERROR(0/0)
0	463.52808	3.0
1	351.02710	3.9
2	283.23364	4.3
3	233.18773	4.8
4	186.09500	5.3
5	139.27782	5.9
6	100.47435	7.0
7	77.37817	6.9
8	49.72884	8.5
9	24.03671	12.2
10	9.65919	20.4
11	2.05970	67.2

SCATTERING OF 7.54 +OR-0.06 MEV NEUTRONS FROM W

LEVEL (S) 0.0 MEV KET (14) 17 ANGLES
0.100
0.111
0.123

ANGLE CM	X-SEC. MB/STR	ERROR (0/0) +	ERROR (0/0) -	RUN
MULTIPLE SCATTERING CORRECTION DONE				
15.09	3554.19	4.5	4.0	50525
22.62	1448.98	5.2	6.4	30525
27.64	539.10	6.6	5.4	50111
35.18	143.97	10.5	7.9	30111
42.71	208.13	7.2	6.8	10111
47.73	223.48	6.5	7.0	50110
55.26	156.73	8.8	7.7	30110
62.78	60.03	12.4	11.9	10110
70.30	37.94	18.3	12.6	50107
77.81	65.07	12.5	8.6	30107
85.31	72.12	10.3	7.6	10107
92.81	67.27	12.2	7.6	50102
100.31	42.39	14.4	9.7	30102
107.80	21.45	17.9	14.7	10102
119.77	20.64	23.9	17.1	50099
127.25	22.23	26.4	12.6	30099
134.73	26.45	14.4	14.2	10099

AVERAGE X-SEC 0.0 MB/STR 0 NOTE

INTEGRATED X-SEC 2813.24 MB ERROR 7.5 PER CENT

P12 FIT

L	COEF.	ERROR (0/0)
0	447.74219	2.6
1	348.54272	3.1
2	287.14600	3.5
3	238.80681	3.8
4	200.20261	4.0
5	162.08463	4.4
6	125.31064	4.6
7	101.31007	5.1
8	74.65388	5.3
9	45.94987	7.0
10	21.71886	11.4
11	7.99819	20.9
12	2.27529	51.6

SCATTERING OF 8.56 +OR-0.06 MEV NEUTRONS FROM W

LEVEL (S) 0.0 MEV KEY (14) 21 ANGLES
0.100
0.111
0.123

MULTIPLE SCATTERING CORRECTION DONE

ANGLE CM	X-SEC. MB/STR	ERROR (0/0) +	ERROR (0/0) -	RUN
10.06	4975.68	4.9	8.3	50554
15.09	3379.45	5.4	7.0	50548
22.62	1219.54	6.8	8.6	30548
27.65	359.12	8.1	9.2	50204
31.67	140.78	11.6	8.5	50321
35.18	133.58	10.0	8.4	30204
39.20	187.40	9.5	7.0	30321
42.72	241.94	7.3	7.9	10204
46.72	239.40	8.5	6.1	10321
47.73	266.93	8.8	5.7	50267
55.26	168.42	8.7	6.5	30267
62.78	57.28	14.3	6.7	10267
70.29	43.09	11.6	8.9	50234
77.80	71.79	9.3	8.3	30234
85.32	81.56	13.6	8.2	10234
92.81	64.30	12.0	13.1	50285
100.31	31.06	14.2	10.3	30285
107.80	19.40	13.9	14.6	10285
119.77	24.59	14.6	17.5	50239
127.25	23.74	14.8	21.9	30239
134.73	21.22	16.4	18.4	10239

AVERAGE X-SEC 0.0 MB/STR 0 NOTE

INTEGRATED X-SEC 2632.13 MB ERROR 7.5 PER CENT

P13 FIT

L	COEF.	ERROR (0/0)
0	418.91699	2.8
1	326.69092	3.3
2	260.81812	3.9
3	218.84288	4.3
4	185.71191	4.5
5	153.97954	4.7
6	125.28264	4.8
7	102.55858	4.8
8	82.04819	5.0
9	54.11766	5.9
10	27.88792	9.2
11	11.61932	16.6
12	4.43031	31.9
13	1.37465	63.3

SCATTERING OF 6.44 +OR-0.07 MEV NEUTRONS FROM W

CONTINUUM X-SEC AVERAGE OF 12 SPECTRA 50 LINES

EN(LAB) MEV	CN MEV	X-SEC MB/STR/MEV	ERROR MB/STR/MEV
3.287	-3.100	9.7	6.0
3.262	-3.125	11.2	6.0
3.237	-3.150	9.8	5.6
3.212	-3.175	9.6	5.6
3.188	-3.200	13.1	5.6
3.163	-3.225	14.3	5.6
3.138	-3.250	13.4	5.6
3.113	-3.275	15.5	5.2
3.088	-3.300	11.4	4.0
3.063	-3.325	10.5	3.6
3.038	-3.350	11.7	3.6
3.014	-3.375	11.7	3.6
2.989	-3.400	15.8	3.6
2.964	-3.425	15.2	3.6
2.939	-3.450	13.9	3.2
2.914	-3.475	14.6	3.6
2.889	-3.500	9.4	2.8
2.864	-3.525	10.4	2.8
2.839	-3.550	13.3	3.2
2.815	-3.575	14.7	2.8
2.790	-3.600	13.8	2.8
2.765	-3.625	13.2	2.8
2.740	-3.650	14.8	2.8
2.715	-3.675	15.2	2.8
2.690	-3.700	12.6	2.4
2.665	-3.725	12.8	2.4
2.641	-3.750	14.9	2.4
2.616	-3.775	18.0	2.4
2.591	-3.800	19.4	2.8
2.566	-3.825	19.1	2.8
2.541	-3.850	18.3	2.8
2.516	-3.875	17.4	2.8
2.491	-3.900	18.6	2.8
2.467	-3.925	21.5	2.8
2.442	-3.950	23.5	2.8
2.417	-3.975	24.4	2.8
2.392	-4.000	24.9	2.8
2.367	-4.025	25.9	2.8
2.342	-4.050	28.0	3.2
2.317	-4.075	29.2	3.2
2.292	-4.100	28.8	3.2
2.268	-4.125	28.5	3.2
2.243	-4.150	28.8	3.2
2.218	-4.175	30.3	3.2
2.193	-4.200	32.8	3.2
2.168	-4.225	34.9	3.6
2.143	-4.250	36.2	3.6
2.118	-4.275	36.1	3.6
2.094	-4.300	36.3	3.6
2.069	-4.325	36.4	3.6

SCATTERING OF 6.44 +OR-0.07 MEV NEUTRONS FROM W

CONTINUUM X-SEC AVERAGE OF 12 SPECTRA 38 LINES

EN (LAB) MEV	CN MEV	X-SEC MB/STR/MEV	ERROR MB/STR/MEV
2.044	-4.350	37.5	3.6
2.019	-4.375	39.6	3.6
1.994	-4.400	40.1	4.0
1.969	-4.425	38.6	3.6
1.944	-4.450	37.9	3.6
1.920	-4.475	39.8	4.0
1.895	-4.500	43.8	4.0
1.870	-4.525	45.8	4.0
1.845	-4.550	45.5	4.4
1.820	-4.575	47.1	4.4
1.795	-4.600	49.8	4.4
1.770	-4.625	53.2	4.8
1.745	-4.650	55.7	4.8
1.721	-4.675	57.2	5.2
1.696	-4.700	56.5	5.2
1.671	-4.725	53.8	5.2
1.646	-4.750	52.4	5.2
1.621	-4.775	54.6	5.2
1.596	-4.800	60.4	5.6
1.571	-4.825	65.6	6.0
1.547	-4.850	68.9	6.4
1.522	-4.875	69.6	6.8
1.497	-4.900	69.7	7.2
1.472	-4.925	71.1	7.2
1.447	-4.950	73.9	8.0
1.422	-4.975	78.2	8.4
1.397	-5.000	78.2	8.8
1.372	-5.025	77.9	9.2
1.348	-5.050	81.6	10.0
1.323	-5.075	90.5	11.2
1.298	-5.100	95.2	12.4
1.273	-5.125	95.2	13.2
1.248	-5.150	98.4	14.0
1.223	-5.175	99.9	14.8
1.198	-5.200	99.2	15.6
1.174	-5.225	108.0	18.8
1.149	-5.250	101.1	20.4
1.124	-5.275	117.4	25.6

SCATTERING OF 7.54 +OR-0.06 MEV NEUTRONS FROM W

CONTINUUM X-SEC AVERAGE OF 13 SPECTRA 50 LINES

EN(LAB) MEV	QN MEV	X-SEC MB/STR/MEV	ERROR MB/STR/MEV
3.629	-3.850	16.5	10.4
3.604	-3.875	22.2	10.0
3.579	-3.900	10.4	7.2
3.555	-3.925	9.5	5.6
3.530	-3.950	9.1	5.2
3.505	-3.975	10.0	4.4
3.480	-4.000	11.8	4.4
3.455	-4.025	11.6	4.4
3.430	-4.050	8.5	4.4
3.405	-4.075	7.4	4.8
3.381	-4.100	9.0	5.2
3.356	-4.125	6.3	4.0
3.331	-4.150	9.4	4.4
3.306	-4.175	10.3	4.0
3.281	-4.200	11.9	4.4
3.256	-4.225	13.8	4.0
3.231	-4.250	11.4	3.6
3.206	-4.275	8.6	3.6
3.182	-4.300	9.6	4.0
3.157	-4.325	8.5	4.0
3.132	-4.350	9.6	4.0
3.107	-4.375	10.5	3.6
3.082	-4.400	12.4	3.6
3.057	-4.425	16.2	4.0
3.032	-4.450	13.7	3.6
3.008	-4.475	10.4	3.2
2.983	-4.500	12.0	3.6
2.958	-4.525	13.0	3.6
2.933	-4.550	16.5	3.6
2.908	-4.575	16.8	3.2
2.883	-4.600	16.0	3.6
2.858	-4.625	17.2	3.2
2.834	-4.650	17.7	3.2
2.809	-4.675	15.8	3.2
2.784	-4.700	15.6	3.6
2.759	-4.725	15.7	3.6
2.734	-4.750	18.0	3.6
2.709	-4.775	22.6	3.6
2.684	-4.800	23.5	4.0
2.659	-4.825	18.1	3.6
2.635	-4.850	17.9	3.6
2.610	-4.875	21.6	3.6
2.585	-4.900	25.6	3.6
2.560	-4.925	24.8	3.6
2.535	-4.950	22.8	4.0
2.510	-4.975	23.7	4.0
2.485	-5.000	26.8	4.0
2.461	-5.025	26.5	4.0
2.436	-5.050	24.8	4.0
2.411	-5.075	27.0	4.0

SCATTERING OF 7.54 +OR-0.06 MEV NEUTRONS FROM W

CONTINUUM X-SEC AVERAGE OF 13 SPECTRA 50 LINES

EN(LAB) MEV	CN MEV	X-SEC MB/STR/MEV	ERROR MB/STR/MEV
2.386	-5.100	32.7	4.4
2.361	-5.125	34.2	4.4
2.336	-5.150	29.2	4.0
2.311	-5.175	27.8	4.4
2.287	-5.200	30.3	4.4
2.262	-5.225	33.6	4.4
2.237	-5.250	32.3	4.4
2.212	-5.275	30.4	4.4
2.187	-5.300	35.3	4.4
2.162	-5.325	40.4	4.4
2.137	-5.350	37.9	4.4
2.112	-5.375	33.1	4.4
2.088	-5.400	33.0	4.4
2.063	-5.425	39.1	4.8
2.038	-5.450	45.7	4.8
2.013	-5.475	47.0	4.8
1.988	-5.500	46.2	4.8
1.963	-5.525	44.4	5.2
1.938	-5.550	46.8	5.2
1.914	-5.575	53.1	5.6
1.889	-5.600	57.9	5.6
1.864	-5.625	54.2	5.6
1.839	-5.650	46.6	5.2
1.814	-5.675	46.5	5.2
1.789	-5.700	53.2	5.6
1.764	-5.725	61.3	6.0
1.740	-5.750	61.0	6.0
1.715	-5.775	59.2	6.0
1.690	-5.800	63.1	6.4
1.665	-5.825	66.3	6.4
1.640	-5.850	69.2	6.8
1.615	-5.875	69.8	6.8
1.590	-5.900	71.6	7.2
1.565	-5.925	72.5	7.6
1.541	-5.950	71.2	7.6
1.516	-5.975	70.5	8.0
1.491	-6.000	71.5	8.4
1.466	-6.025	71.1	8.4
1.441	-6.050	72.4	8.8
1.416	-6.075	79.3	9.6
1.391	-6.100	86.6	10.4
1.367	-6.125	86.2	10.8
1.342	-6.150	81.5	11.2
1.317	-6.175	83.4	11.6
1.292	-6.200	92.5	13.2
1.267	-6.225	100.8	14.8
1.242	-6.250	101.5	15.2
1.217	-6.275	98.6	15.6
1.192	-6.300	97.0	16.4
1.168	-6.325	103.9	19.6

SCATTERING OF 8.56 +CR-0.06 MEV NEUTRONS FROM W

CONTINUUM X-SEC AVERAGE OF 15 SPECTRA 50 LINES

EN(LAB) MEV	CN MEV	X-SEC MB/STR/MEV	ERROR MB/STR/MEV
4.340	-4.150	8.3	6.0
4.315	-4.175	10.2	6.0
4.290	-4.200	9.0	4.8
4.265	-4.225	11.6	4.8
4.240	-4.250	11.8	5.2
4.215	-4.275	9.7	5.2
4.191	-4.300	11.4	4.8
4.166	-4.325	10.8	4.8
4.141	-4.350	7.3	4.0
4.116	-4.375	6.2	4.0
4.091	-4.400	6.7	4.0
4.066	-4.425	7.8	4.0
4.041	-4.450	7.8	4.0
4.017	-4.475	9.0	3.2
3.992	-4.500	9.6	3.6
3.967	-4.525	8.3	3.6
3.942	-4.550	11.0	4.0
3.917	-4.575	11.6	4.0
3.892	-4.600	9.0	3.6
3.867	-4.625	7.5	3.6
3.842	-4.650	7.0	3.6
3.818	-4.675	7.7	3.2
3.793	-4.700	11.4	3.2
3.768	-4.725	10.9	2.8
3.743	-4.750	11.3	2.8
3.718	-4.775	11.9	2.8
3.693	-4.800	12.5	2.8
3.668	-4.825	13.1	2.8
3.644	-4.850	9.5	2.8
3.619	-4.875	10.2	2.8
3.594	-4.900	12.1	2.8
3.569	-4.925	11.7	2.4
3.544	-4.950	12.6	2.8
3.519	-4.975	10.7	2.8
3.494	-5.000	12.2	2.8
3.470	-5.025	10.5	2.8
3.445	-5.050	12.6	2.8
3.420	-5.075	14.8	2.8
3.395	-5.100	18.0	2.8
3.370	-5.125	19.0	2.8
3.345	-5.150	16.1	2.8
3.320	-5.175	13.4	2.8
3.295	-5.200	14.9	2.8
3.271	-5.225	17.8	2.8
3.246	-5.250	18.6	2.8
3.221	-5.275	16.4	2.8
3.196	-5.300	14.6	2.8
3.171	-5.325	16.7	2.8
3.146	-5.350	16.9	2.8
3.121	-5.375	15.2	2.8

SCATTERING OF 8.56 +OR-0.06 MEV NEUTRONS FROM W

CONTINUUM X-SEC AVERAGE OF 15 SPECTRA 50 LINES

EN(LAB) MEV	QN MEV	X-SEC MB/STR/MEV	ERROR MB/STR/MEV
3.097	-5.400	13.4	2.8
3.072	-5.425	18.2	2.8
3.047	-5.450	23.4	2.8
3.022	-5.475	25.6	2.8
2.997	-5.500	23.3	3.2
2.972	-5.525	22.2	3.2
2.947	-5.550	24.6	3.2
2.922	-5.575	26.9	3.2
2.898	-5.600	27.7	3.2
2.873	-5.625	27.7	3.2
2.848	-5.650	28.2	3.2
2.823	-5.675	26.6	3.2
2.798	-5.700	25.0	3.2
2.773	-5.725	24.3	3.2
2.748	-5.750	27.8	3.2
2.724	-5.775	28.1	3.2
2.699	-5.800	27.6	3.2
2.674	-5.825	27.2	3.2
2.649	-5.850	28.8	3.2
2.624	-5.875	31.3	3.2
2.599	-5.900	33.0	3.6
2.574	-5.925	32.1	3.2
2.550	-5.950	33.3	3.6
2.525	-5.975	34.9	3.6
2.500	-6.000	35.0	3.6
2.475	-6.025	32.7	3.6
2.450	-6.050	31.7	3.6
2.425	-6.075	34.1	3.6
2.400	-6.100	36.8	3.6
2.375	-6.125	37.1	3.6
2.351	-6.150	35.8	3.6
2.326	-6.175	35.2	3.6
2.301	-6.200	36.9	3.6
2.276	-6.225	41.1	4.0
2.251	-6.250	43.0	4.0
2.226	-6.275	41.6	4.0
2.201	-6.300	40.8	4.0
2.177	-6.325	42.1	4.0
2.152	-6.350	45.7	4.0
2.127	-6.375	49.4	4.4
2.102	-6.400	52.8	4.4
2.077	-6.425	53.7	4.4
2.052	-6.450	52.4	4.4
2.027	-6.475	49.2	4.4
2.003	-6.500	47.8	4.4
1.978	-6.525	49.6	4.4
1.953	-6.550	53.3	4.8
1.928	-6.575	55.4	4.8
1.903	-6.600	55.9	4.8
1.878	-6.625	55.9	4.8

SCATTERING OF 8.56 +OR-0.06 MEV NEUTRONS FROM W

CONTINUUM X-SEC AVERAGE OF 15 SPECTRA 26 LINES

EN(LAB) MEV	CN MEV	X-SEC MB/STR/MEV	ERROR MB/STR/MEV
1.853	-6.650	57.3	5.2
1.828	-6.675	60.2	5.2
1.804	-6.700	63.6	5.6
1.779	-6.725	66.2	5.6
1.754	-6.750	69.4	6.0
1.729	-6.775	72.3	6.0
1.704	-6.800	74.5	6.4
1.679	-6.825	75.1	6.4
1.654	-6.850	77.6	6.8
1.630	-6.875	79.6	6.8
1.605	-6.900	83.3	7.2
1.580	-6.925	86.1	7.6
1.555	-6.950	89.8	8.0
1.530	-6.975	92.3	8.8
1.505	-7.000	92.4	8.8
1.480	-7.025	90.9	9.2
1.456	-7.050	90.6	9.6
1.431	-7.075	93.6	10.0
1.406	-7.100	96.3	10.4
1.381	-7.125	98.8	11.2
1.356	-7.150	103.2	12.4
1.331	-7.175	110.8	13.6
1.306	-7.200	116.2	15.2
1.281	-7.225	113.9	15.2
1.257	-7.250	112.0	16.0
1.232	-7.275	124.8	18.0

ORNL-4803
UC-34 — Physics

INTERNAL DISTRIBUTION

1-3. Central Research Library
4. ORNL — Y-12 Technical Library
Document Reference Section
5-54. Laboratory Records Department
55. Laboratory Records, ORNL R.C.
56-58. L. S. Abbott
59. R. G. Alsmiller, Jr.
60. C. E. Clifford
61. F. L. Culler
62. J. K. Dickens
63. C. Y. Fu
64. W. O. Harms
65-74. W. E. Kinney
75. T. A. Love
76-78. F. C. Maienschein
79. G. L. Morgan
80. F. R. Mynatt
81. E. M. Oblow
82. R. W. Peelle
83. S. K. Penny
84-98. F. G. Perey
99. R. W. Roussin
100. M. J. Skinner
101. A. M. Weinberg
102. H. Feshbach (consultant)
103. P. F. Fox (consultant)
104. C. R. Mehl (consultant)
105. H. T. Motz (consultant)

EXTERNAL DISTRIBUTION

106. M. Drake, Brookhaven National Laboratory, Upton, L.I., New York 11973
107. Norman Francis, Knolls Atomic Power Laboratory, General Electric, Schenectady, New York 12309
108. Martin P. Fricke, Gulf Radiation Technology, P.O. Box 608, San Diego, California 92112
109. M. D. Goldberg, Brookhaven National Laboratory, Upton, L.I., New York 11973
110. H. Goldstein, Columbia University, 287A Engineering Terrace Building, 520 W. 120th St., New York 10027
111. W. H. Hannum, Division of Reactor Development and Technology, AEC, Washington, D.C. 20546
112. P. B. Hemmig, Division of Reactor Development and Technology, AEC, Washington, D.C. 20546
113. C. E. Hollandsworth, USA Nuclear Effects Lab., Aberdeen Proving Ground, Maryland
114. J. C. Hopkins, Los Alamos Scientific Laboratory, Los Alamos, New Mexico 87544
115. R. L. Howerton, Lawrence Radiation Laboratory, Livermore, California 94550
116. Capt. Dean Kaul, Department of Defense, Defense Nuclear Agency, Washington, D.C. 20305
117. Kermit Laughon, AEC Site Representative, ORNL
118. M. T. McEllistrem, University of Kentucky, Lexington, Kentucky 40506
119. Vic Orphan, Gulf Radiation Technology, P.O. Box 608, San Diego, California 92112
120. S. Pearlstein, Brookhaven National Laboratory, National Neutron Cross Section Center, Upton, L.I., New York 11973

121. A. B. Smith, Argonne National Laboratory, Argonne, Illinois 60440
122. Leona Stewart, Los Alamos Scientific Laboratory, Los Alamos, New Mexico 87544
123. J. J. Schmidt, Head, Nuclear Data, IAEA, Karntner, Ring 11, A-1010, Vienna, Austria
124. J. A. Swartout, Union Carbide Corporation, New York, N.Y. 10017
125. W. E. Tucker, Texas Nuclear Corporation, 5805 Bullard Drive, Austin, Texas 78731
126. Phil Young, Los Alamos Scientific Laboratory, Los Alamos, New Mexico 87544
127. Research and Technical Support Division, AEC, ORO
128. Patent Office, AEC, ORO

129-356. Given distribution as shown in TID-4500 under Physics category (25 copies — NTIS)